Supporting Information

In-Situ ^{27}Al NMR Spectroscopy of Aluminate in Sodium Hydroxide Solutions Above and Below Saturation with Respect to Gibbsite

Trent R. Graham[a], Mateusz Dembowski[b], Ernesto Martinez-Baez[c], Xin Zhang[b], Nicholas R. Jaegers[a], Jianzhi Hu[b], Miroslaw S. Gruszkiewicz[d], Hsiu-Wen Wang[d], Andrew G. Stack[d], Mark E. Bowden[b], Calvin H. Delegard[e], Gregory K. Schenter[b], Aurora E. Clark[c], Sue B. Clark[b,c], Andrew R. Felmy[b,c], Kevin M. Rosso[b], Carolyn I. Pearce[b*]

[a] *The Voiland School of Chemical and Biological Engineering and* [c] *Department of Chemistry, Washington State University, Pullman, Washington 99164, United States*

[b] *Pacific Northwest National Laboratory, Richland, Washington 99352, United States*

[d] *Oak Ridge National Laboratory, Oak Ridge, Tennessee 37831, United States*

[e] *TradeWind Services LLC, Richland, Washington 99352, United States*

T. R. G. and M. D. contributed equally

Corresponding Author

* carolyn.pearce@pnnl.gov Phone: +1 (509) 372–4875

Table of Contents

Experimental Methodology

Raman Spectroscopy.

Raman spectroscopy measurements were performed on filtered solutions using a Horiba LabRam HR spectrometer equipped with an inverted optical microscope (Nikon Ti-E, 10x microscope objective). Continuous laser light source (633 nm) was used to collect spectra in the 100 – 4000 cm^{-1} range using ten, ten second exposure times at 4 cm^{-1} resolution. The data was baseline corrected with a linear function between 400 and 800 cm^{-1}.

Powder X-ray Diffraction

Patterns were collected on a Philips X'pert Multi-Purpose diffractormeter (MPD) (PANAlytical, Almelo, The Netherlands) using a fixed Cu anode operating at 50 kV and 40 mA. The 2θ values were varied between 10 - 80°. Phases were identified using JADE 9.5.1 (Materials Data Inc.), and with the 2012 PDF4+ database from the International Center for Diffraction Data (ICDD). The calculation of crystal domain size was performed in Topaz (v.5).

Scanning Electron Microscopy

Micrographs were collected on a Helios NanoLab 600i SEM (FEI, Hillsboro, OR). The samples were sputter coated with 5 nm of carbon. Micrographs were processed in ImageJ, wherein at least 30 nanoparticles were counted for length measurements, and 50 nanoparticles were counted for thickness measurements for each sample.

Inductively Coupled Plasma Optical Emission Spectroscopy

Elemental concentrations were determined on nitric acid acidified samples with a Perkin Elmer Optima 2100 DV ICP-OES with an AS93 auto sampler. A Helix Tracey 4300 DV spray chamber and SeaSpray nebulizer were used with double distilled 2 % nitric acid (GFS Chemicals, Inc. Cat. 621) and a flow rate of 1.5 mL/min. Calibration standards were made with Ultra Scientific ICP standards (Kingstown, RI) in a diluted range of 0.5 to 3000 μg/L.

PHREEQC

Model Description

This new calculation for activity coefficients and mineral solubility for the system of Na^+-$Al(OH)_4^-$-OH^--NO_3^- has been made using the Pitzer virial-coefficient approach and literature data for activity coefficient corrections and interaction parameters. This takes the form of a database for the PHREEQC software package (version 3) that augments the default *pitzer.dat*. The database consists of additional information regarding the

(1) Selected aqueous Al- and N-containing species, with their valence states +3 and -5 and solution master species as Al^{3+} and NO_3^-.

(2) Solution species with their formation reaction equilibrium constants, including the Al species of Al^{3+}, $Al(OH)_4^-$, $AlOH^{2+}$, $Al(OH)_2^+$, $Al(OH)_3^0$, and the N species of NO_3^- and $NaNO_3^0$. With the exception of the $NaNO_3^0$ (the neutral sodium nitrate), all species, including the temperature-dependence of their formation equilibrium constants, were transferred from the existing *phreeqc.dat* database, but leaving out their activities (-*gamma*), which are now calculated from the Pitzer model. The association equilibrium constant temperature-dependencies for $NaNO_3^0$ were calculated from the reduced chemical potentials of formation of the species given by Reynolds *et al.*[1] (in their Table 2).

(3) Gibbsite, bayerite and boehmite solid phases were added with the solubility product equilibrium constant temperature-dependence from Bénézeth *et al.*[2] (for gibbsite and bayerite) and Xiong[3] (for boehmite).

(4) Parameters for the Pitzer ion-interaction aqueous model implemented in PHREEQC. The coefficients were included as follows:

   a. Binary cation-anion interaction parameters β^0, β^1, and C^Φ for Na^+/OH^-,[3,4] $Na^+/Al(OH)_4^-$,[4,5] and Na^+/NO_3^-.[1,4]

   b. Mixed binary anion-anion interaction parameters θ for NO_3^-/OH^-,[1,4] NO_3^-/Cl^-,[4] $Al(OH)_4^-/OH^-$,[5] and $Al(OH)_4^-/NO_3^-$.[5]

   c. Mixed ternary interaction parameters Ψ for $Na^+/Cl^-/Al(OH)_4^-$,[3,6] $Na^+/OH^-/Al(OH)_4^-$,[5] $Na^+/NO_3^-/Al(OH)_4^-$,[4] $Na^+/Cl^-/OH^-$,[4] and $Na^+/NO_3^-/OH^-$.[1,4]

   d. Binary ion-neutral interaction parameters λ for $NaNO_3^0/OH^-$.[1]

   e. Ternary cation-anion-neutral interaction parameters ζ for $Na^+/OH^-/NaNO_3^0$.[1]

All equilibrium constants and Pitzer parameters were the best values selected from the literature, with the temperature dependence if available. The results should be reasonably accurate between ambient temperature and 100 °C, and are verified by comparing results calculated from PHREEQC with the literature data (e.g., Figs. S1 and S2). It should be kept in mind that, here, literature data have been regressed from experimental results of limited accuracies and ranges, often using data obtained by others. For this reason, there is some correlation between the parameters and as a result sometimes replacing some parameters with a possibly more accurate set of may lead to a worse representation. The input data block (tabulated below) is still under the development to include further phases beyond gibbsite. Readers who are interested in the future update can send the request to the corresponding author.

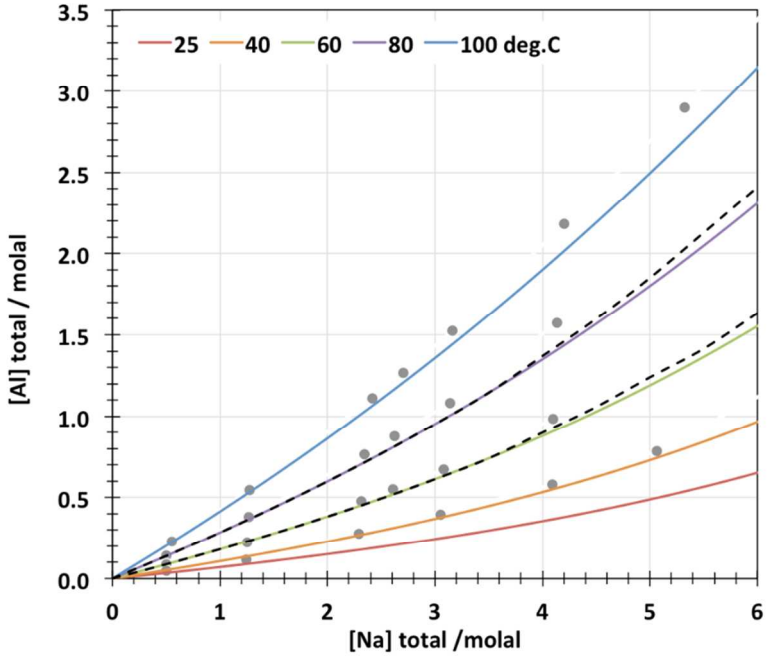

Figure S1. Solubility of gibbsite in the $Al(OH)_3$-NaOH-H_2O system. The solubility calculations from PHREEQC agree very well with results reported by Russell *et al.*[7] (gray spheres), which represents an independent test. The results also show good agreement with the solubility model by Königsberger *et al.*[6] (black dash curves). Königsberger *et al.*'s model is constructed based on extension of Wesolowski[5] Pitzer treatment of gibbsite solubility in 0-5 molal of NaCl+NaOH solutions.

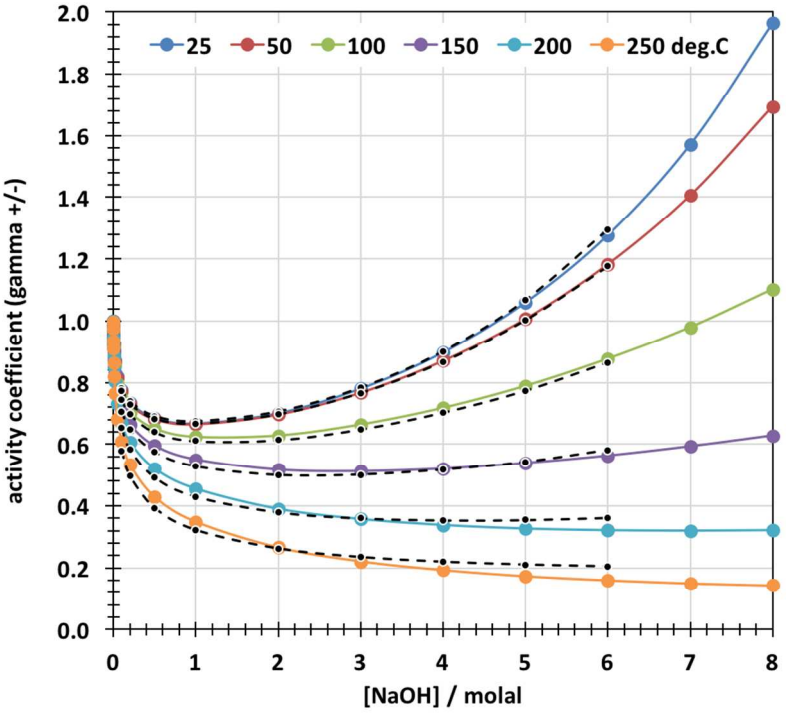

Figure S2. Calculated activity coefficients based on Xiong[3] compared with the experimental data (black dash curves) listed by Holmes and Mesmer,[8] which are also consistent with Simonson *et al.*[9]

PHREEQC input data block

```
DATABASE pitzer.dat       # must use DATABASE pitzer.dat
TITLE Pitzer activity coefficients etc.

SOLUTION_MASTER_SPECIES
Al              Al+3            0       Al              26.9815
Al(+3)          Al+3            0       Al
N               NO3-            0       N               14.0067
N(+5)           NO3-            0       N

SOLUTION_SPECIES
Al+3 = Al+3
        -dw         0.559e-9
        -Vm         -2.28  -17.1  10.9  -2.07  2.87  9  0  0  5.5e-3  1
Al+3 + 4 H2O = Al(OH)4- + 4 H+
        -log_k      -22.7
        -delta_h 42.30          kcal
        -analytic   51.578      0.0         -11168.9    -14.865
Al+3 + H2O = AlOH+2 + H+
        -log_k      -5.0
        -delta_h 11.49          kcal
        -analytic   -38.253     0.0         -656.27     14.327
        -Vm         -1.46  -11.4  10.2  -2.31  1.67  5.4  0  0  0  1
Al+3 + 2 H2O = Al(OH)2+ + 2 H+
        -log_k      -10.1
        -delta_h 26.90          kcal
        -analytic   88.50       0.0         -9391.6     -27.121
Al+3 + 3 H2O = Al(OH)3 + 3 H+
        -log_k      -16.9
        -delta_h 39.89          kcal
        -analytic   226.374     0.0         -18247.8    -73.597
NO3- = NO3-
        -dw         1.9e-9
        -Vm         6.32  6.78  0  -3.06  0.346  0  0.93  0  -0.012  1
NO3- + Na+ = NaNO3      # Reynolds_2015
        -analytic -9.632157103   -0.006230388637   -183.03701404   4.692610000

PHASES
Gibbsite
        Al(OH)3 + OH-  = Al(OH)4-
        -delta_h  22.5 kJ
        -analytic  -96.5506    -0.0139828   2374.88   37.023242684          # Benezeth_2016
Bayerite
        Al(OH)3 + OH-  = Al(OH)4-
        -delta_h  18.9 kJ
        -analytic  -96.9332    -0.0139828   2562.14   37.023242684          # Benezeth_2016
#       -analytic  -96.9242    -0.0139828   2583.87   37.023242684          # Benezeth_2016 SIT
Boehmite
        AlOOH + 2 H2O = Al(OH)4- + H+
#       -analytic  -5.991052   0.0  -2598.755                               # Palmer_2001 in Xiong_2014
        -analytic  -6.082542   0.0  -2526.286                               # Xiong_2014

PITZER
#some parameters were regressed using a set of other parameters and therefore may be dependent on #these specific values of other parameters to reproduce data
        -macinnes   false
        -redox      false
-B0
Na+             OH-   0.0869   -356.02   -1.0814                                          # Weber_2001
#   Na+         OH-   0.0883443913   -1197.84571   -6.10983033   0.00743325156# Xiong_2014
    Na+         Al(OH)4-   0.0513   -356.02   -1.0814                  # Wesolowski_1992 in Weber_2001
#   Na+         NO3-  0.00204  -406.5    -1.04                         # Weber_2001
    Na+         NO3-  0.028327  1406.73   10.51503   -0.01831          # Reynolds_2015

-B1
Na+             OH-   0.2481    173.16   1.2073                                           # Weber_2001
#   Na+         OH-   0.244421177    1627.02502   9.48250496    -0.0115788697   # Xiong_2014
    Na+         Al(OH)4-   0.2481    173.16   1.2073                   # Wesolowski_1992 in Weber_2001
#   Na+         NO3-  0.2368   -712.4   -1.214                          # Weber 2001
    Na+         NO3-  0.330682   0.   0.   0.004124                    # Reynolds_2015
```

```
    -C0
    Na+             OH-   0.0039    34.22    0.0842                                                  # Weber_2001
#   Na+             OH-   0.00399943679   88.2475511   0.406876285  -0.000475666912          # Xiong_2014
    Na+             Al(OH)4-   0.0013    34.22    0.0842                  # Wesolowski_1992 in Weber_2001
#   Na+      NO3-  0.00008   27.22    0.0756                               # Weber_2001
    Na+             NO3-  0.   0.   0.   0.                               # Reynolds_2015

    -THETA
#   OH-             Cl-    -0.05          # Weber_2001 already in PITZER.dat
#   NO3-                    OH-    -0.0547                  # Weber_2001
    NO3-                    OH-    -0.092138                # Reynolds_2015
    NO3-                    Cl-    0.016                    # Weber_2001
    Al(OH)4-        OH-    0.014                  # Wesolowski_1992
    Al(OH)4-        NO3-   -0.0272                # Wesolowski_1992

    -PSI
    Na+             Cl-         Al(OH)4-   -0.04857  # Xiong_2014
#   Na+             Cl-         Al(OH)4-   -0.055    # Königsberger_2006
    Na+             OH-         Al(OH)4-   -0.0048   # Wesolowski_1992
    Na+             NO3-        Al(OH)4-   0.0047    # Weber_2001
    Na+             Cl-         OH-   -0.0063              # Weber_2001
#   Na+             NO3-        OH-   0.0002               # Weber_2001
    Na+             NO3-        OH-   0.0003629            # Reynolds_2015

    -LAMDA
    NaNO3           OH-   0.114519   0.   0.   -0.0011                  # Reynolds_2015

    -ZETA
    Na+             OH-         NaNO3    -0.00818   0.   0.   0.0000853          # Reynolds_2015
```

Experimental Results

Table S1. Summary of ICP-OES and ^{27}Al NMR results prior to heating.

Sample conditions		**ICP-OES**	**^{27}Al NMR**	
[Al]	[NaOH]	[Al]	δ (ppm)	FWHM (Hz)
0.15	3.00	0.128	80.358	16.40
0.50	3.00	0.277	80.368	22.80
1.00	3.00	0.303	80.370	23.30
2.40	3.00	0.134	80.368	16.50

Table S2. Summary of ICP-OES and ^{27}Al NMR results subsequent to heating.

Sample conditions		**ICP-OES**	**^{27}Al NMR**	
[Al]	[NaOH]	[Al]	δ (ppm)	FWHM (Hz)
0.15	3.00	0.130	80.362	17.20
0.50	3.00	0.416	80.385	32.20
1.00	3.00	0.816	80.416	53.40
2.40	3.00	0.773	80.409	44.30

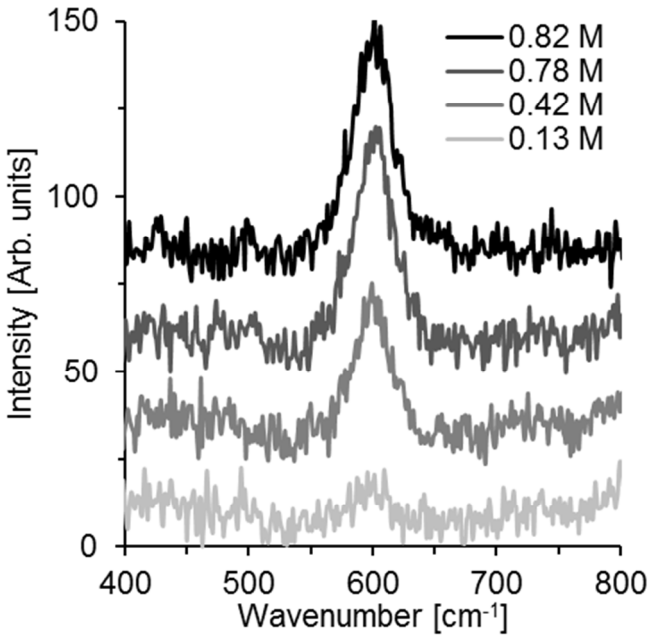

Figure S3. Raman spectra of selected aluminate NMR solutions. The results are consistent with no formation of aluminate dimers.

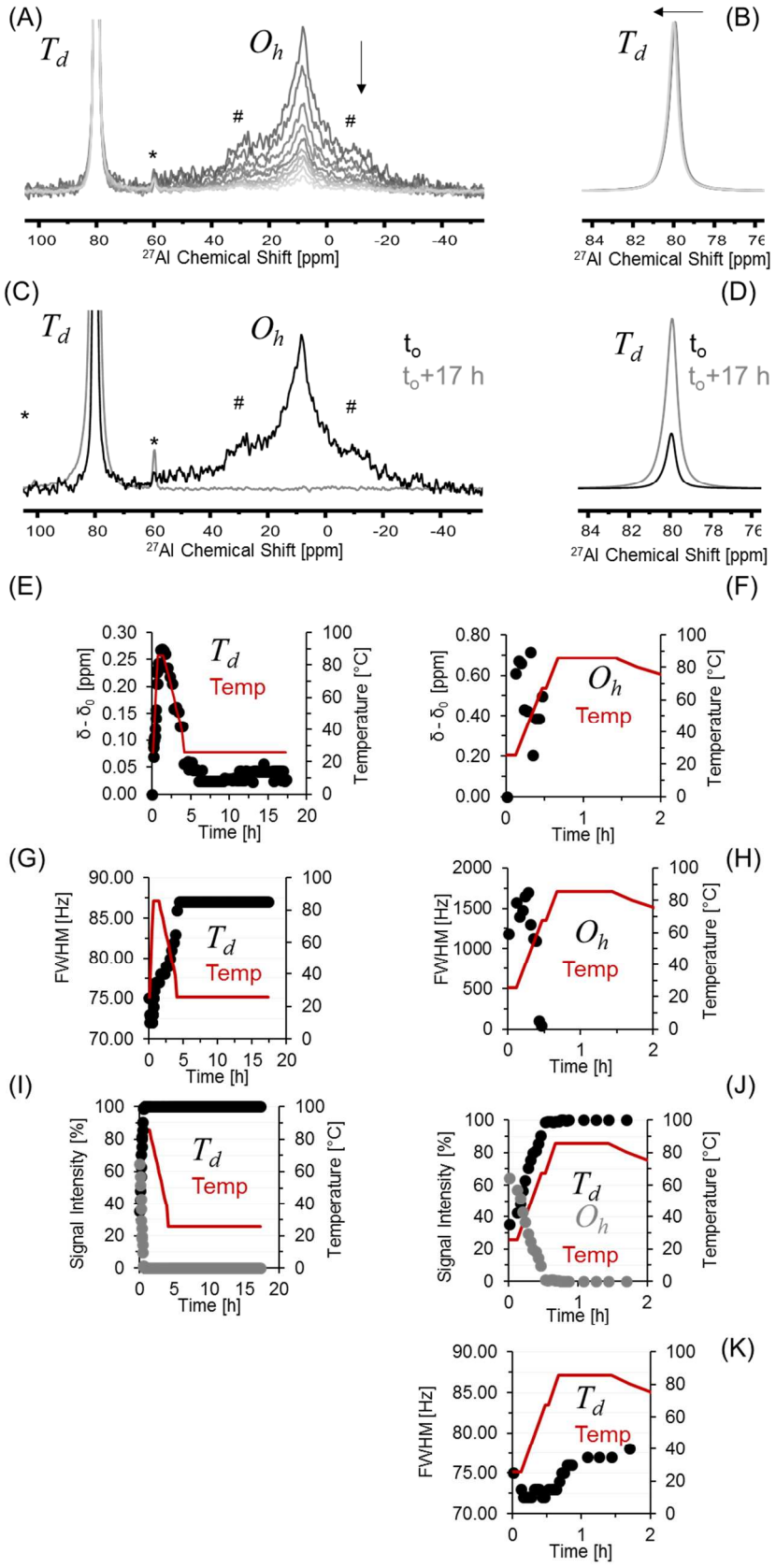

Figure S4. 0.15 M Gibbsite in 3 M NaOH. **(A)** *In-situ* NMR spectra collected during the temperature ramp up to 80 °C with emphasis on the O_h region. The spinning side bands of the T_d resonance (*) and the O_h resonance (#) are delineated. The arrow denotes the progression of time. The spectra are normalized to the height of the T_d resonance. **(B)** *In-situ* NMR spectra during the temperature up to 80 °C with emphasis on the T_d region. The arrow denotes the progression of time. The spectra are normalized to the height of the T_d resonance. **(C)** A comparison of the in-situ NMR spectra acquired at 25°C immediately upon entry into the NMR spectrometer t_0 and the final scan at 25°C after the temperature ramp, with emphasis on the O_h region. The spinning side bands of the T_d resonance (*) and the O_h resonance (#) are delineated. **(D)** A comparison of the *in-situ* NMR spectra acquired at 25°C immediately upon entry into the NMR spectrometer t_0 and the final scan at 25°C after the temperature ramp, with emphasis on the T_d region. **(E)** The change in chemical shift of the T_d resonance, where δ_0 is the initial chemical shift of the T_d resonance. **(F)** The change in chemical shift of the O_h resonance, where δ_0 is the initial chemical shift of the O_h resonance. The first 2 h of the run are shown. **(G)** The full width half maximum (FWHM) of the T_d resonance. **(H)** The FWHM of the O_h resonance. The first 2 h of the run are shown. **(I)** The relative signal intensities of the T_d and O_h resonance. **(J)** The relative signal intensities of the T_d and O_h resonance. The first 2 h of the run are shown. **(K)** The FWHM of the T_d resonance. The first 2 h of the run are shown.

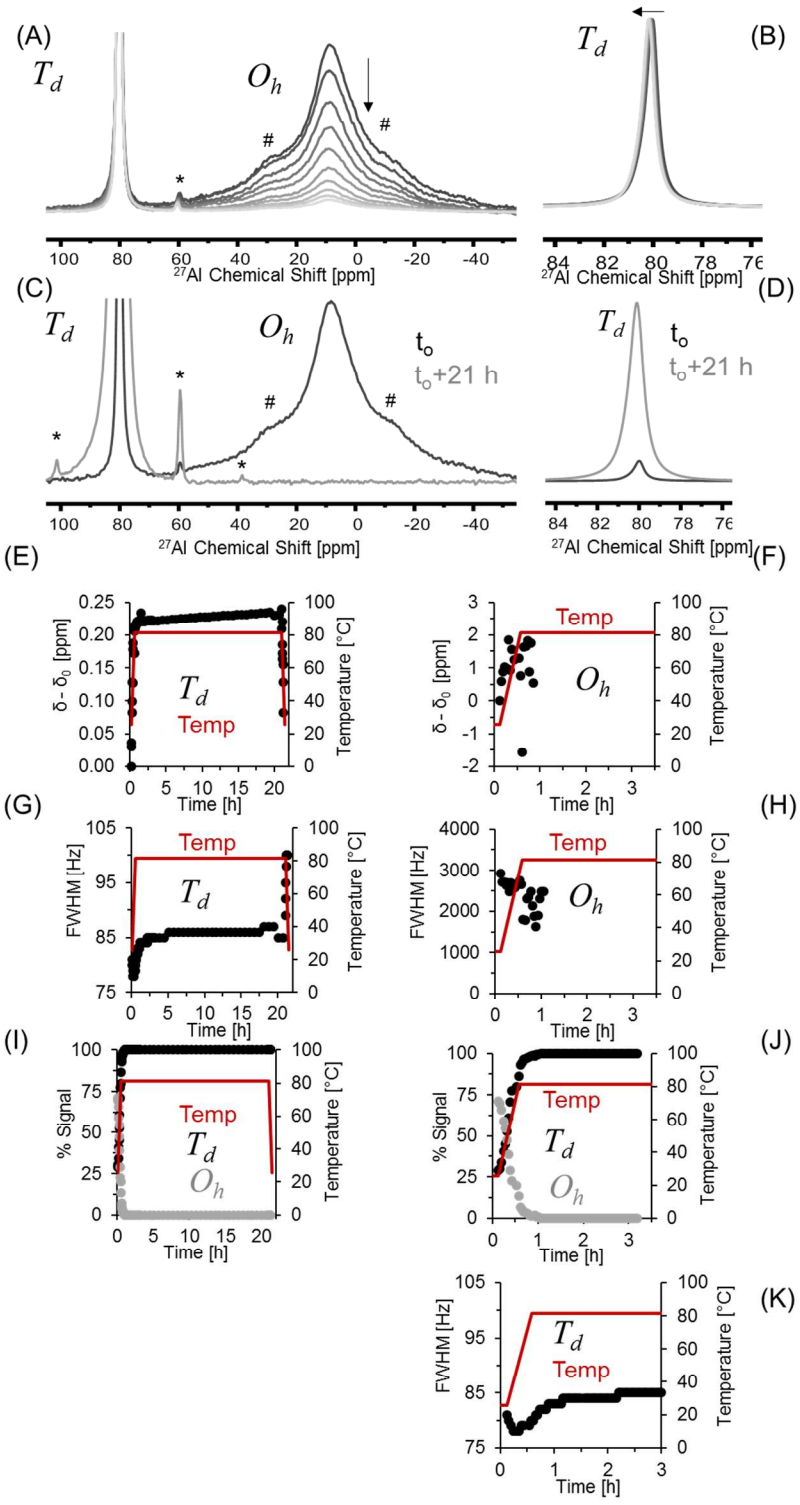

Figure S4. 1.0 M Gibbsite in 3 M NaOH. **(A)** *In-situ* NMR spectra collected during the temperature ramp up to 80 °C with emphasis on the O_h region. The spinning side bands of the T_d resonance (*) and the O_h resonance (#) are delineated. The arrow denotes the progression of time. The spectra are normalized to the height of the T_d resonance. **(B)** *In-situ* NMR spectra during the temperature up to 80 °C with emphasis on the T_d region. The arrow denotes the progression of time. The spectra are normalized to the height of the T_d resonance. **(C)** A comparison of the in-situ NMR spectra acquired at 25°C immediately upon entry into the NMR spectrometer t_0 and the final scan at 25°C after the temperature ramp, with emphasis on the O_h region. The spinning side bands of the T_d resonance (*) and the O_h resonance (#) are delineated. **(D)** A comparison of the *in-situ* NMR spectra acquired at 25°C immediately upon entry into the NMR spectrometer t_0 and the final scan at 25°C after the temperature ramp, with emphasis on the T_d region. **(E)** The change in chemical shift of the T_d resonance, where δ_0 is the initial chemical shift of the T_d resonance. **(F)** The change in chemical shift of the O_h resonance, where δ_0 is the initial chemical shift of the O_h resonance. The first 2 h of the run are shown. **(G)** The full width half maximum (FWHM) of the T_d resonance. **(H)** The FWHM of the O_h resonance. The first 2 h of the run are shown. **(I)** The relative signal intensities of the T_d and O_h resonance. **(J)** The relative signal intensities of the T_d and O_h resonance. The first 2 h of the run are shown. **(K)** The FWHM of the T_d resonance. The first 2 h of the run are shown.

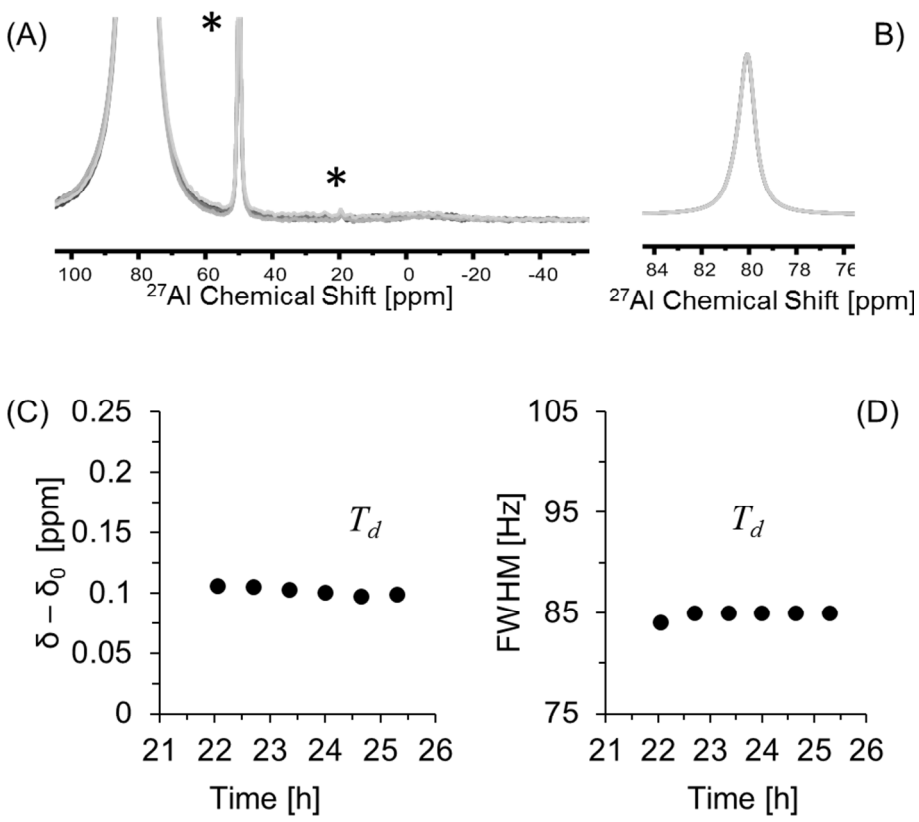

Figure S6. 1.0 M $Al(OH)_3$ in 3 M NaOH (A) *In-situ* NMR spectra collected during the temperature ramp up to 80 °C with emphasis on the O_h region. The spinning side bands of the T_d resonance are delineated. (B) *In-situ* NMR spectra collected during the temperature ramp up to 80 °C with emphasis on the T_d region. (C) The change in chemical shift of the T_d resonance, where δ_0 is the initial chemical shift of the T_d resonance upon entry of the sample to the spectrometer. (D) The full width at half maximum of the T_d resonance.

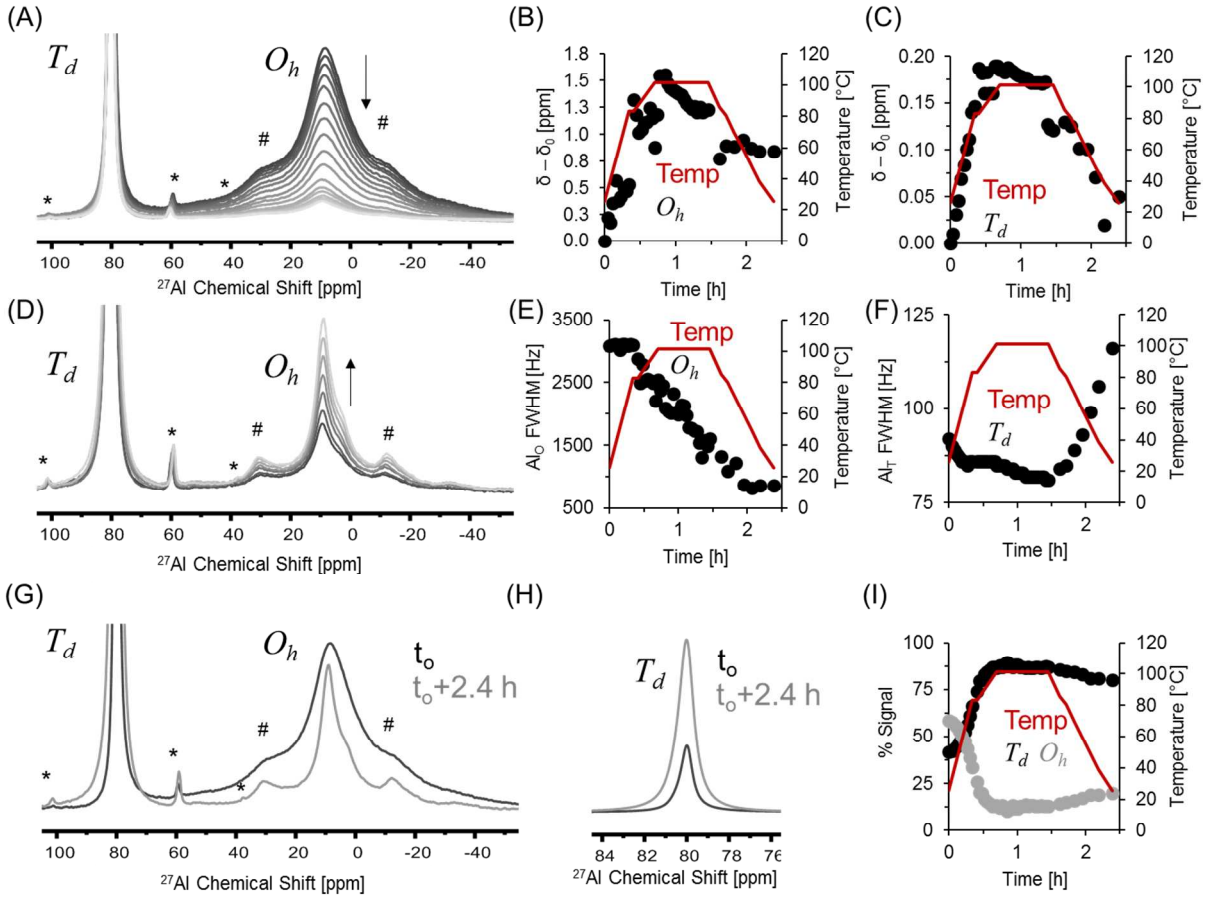

Figure S7. 2.4 M Gibbsite in 3.0 M NaOH **(A)** *In-situ* NMR spectra collected during the temperature ramp up to 100°C with emphasis on the O_h region. The spinning side bands of the T_d resonance (*) and the O_h resonance (#) are delineated. The arrow denotes the progression of time. The spectra are normalized to the height of the T_d resonance. **(B)** The change in chemical shift of the O_h resonance, where δ_0 is the initial chemical shift of the O_h resonance. **(C)** The change in chemical shift of the T_d resonance, where δ_0 is the initial chemical shift of the T_d resonance. **(D)** *In-situ* NMR spectra during the temperature ramp down to 25°C with emphasis on the O_h region. The arrow denotes the progression of time. The spectra are normalized to the height of the T_d resonance. **(G)** A comparison of the in-situ NMR spectra acquired at 25°C immediately upon entry into the NMR spectrometer t_0 and the final scan at 25°C after the temperature ramp, with emphasis on the O_h region. The spinning side bands of the T_d resonance (*) and the O_h resonance (#) are delineated. **(E)** The full width half maximum (FWHM) of the O_h resonance. **(F)** The full width half maximum (FWHM) of the T_d resonance. **(G)** A comparison of the *in-situ* NMR spectra acquired at 25°C immediately upon entry into the NMR spectrometer t_0 and the final scan at 25°C after the temperature ramp, with emphasis on the O_h region. **(H)** A comparison of the *in-situ* NMR spectra acquired at 25°C immediately upon entry into the NMR spectrometer t_0 and the final scan at 25°C after the temperature ramp, with emphasis on the T_d region. **(I)** The relative signal intensities of the T_d and O_h resonance.

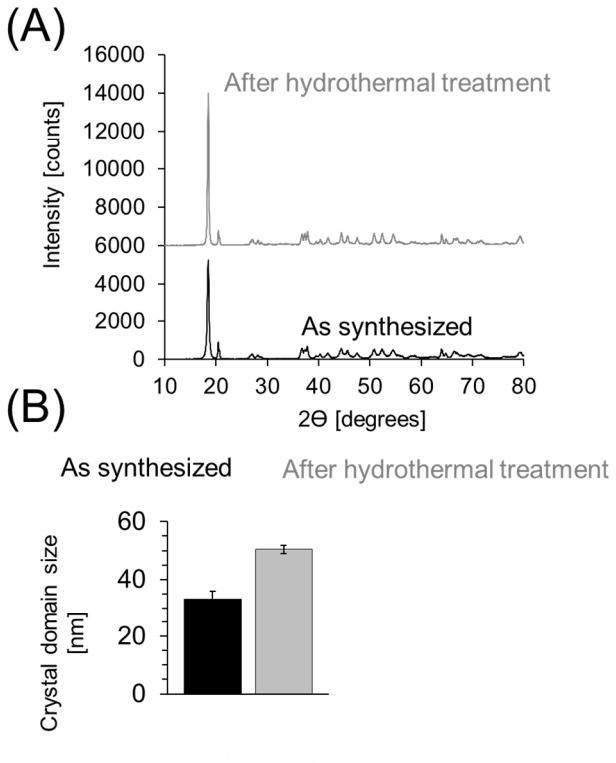

Figure S8. (A) XRD of the as synthesized gibbsite and the gibbsite following brief hydrothermal treatment at 100°C in 3 M NaOH. (B) The crystal domain.

Table S3. ^{27}Al absolute shielding tensor (σ_{Al}) of aluminate ions at discrete distances from Na ions.

Al – Na Separation [Å]	Indirect [ppm]	Direct [ppm]
2.53	529.58 ± 0.34	514.82 ± 0.37
4.11	531.47 ± 0.27	528.85 ± 0.26
6.02	532.14 ± 0.27	531.79 ± 0.30

Reference Simulation: $\langle\sigma_{ref}\rangle = 532.36$; $\bar{s} = 0.30$

The reference simulation absolute shielding tensor calculation was performed on an aluminate ion in the simulation box solvated by 91 waters as shown in Figure S9 D.

Calculation of the difference in chemical shifts utilized Equation S1.[1] We emphasize that the established convention is such that a decrease in the shielding of the analyte (σ_{Al}) with respect to the shielding of the reference corresponds with an increase in chemical shift (δ).

$$\delta = \sigma_{ref} - \sigma_{Al} \tag{S1}$$

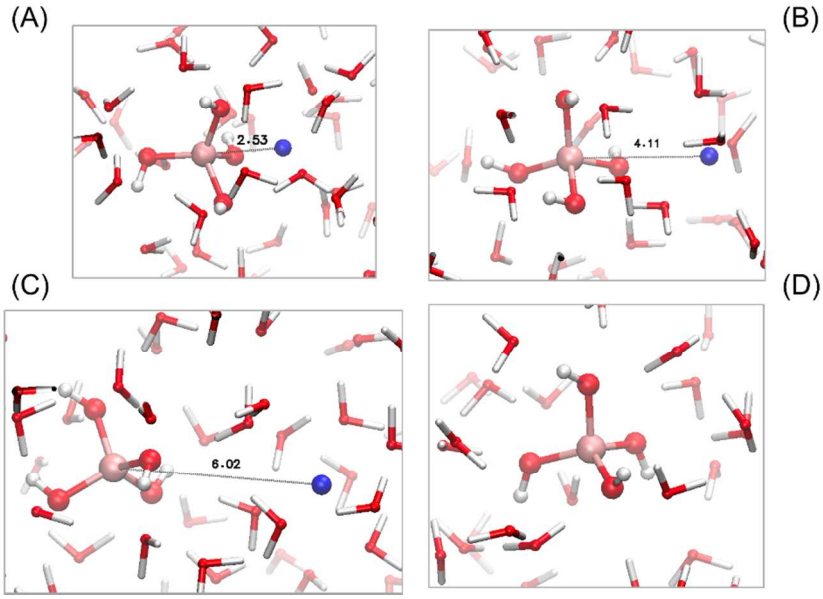

Figure S9. (A) Typical snapshot showing the chemical environment of the aluminate ion with the Na…Al distance of (A) 2.53 (B) 4.11 (C) 6.02 Å and (D) without Na in the simulation.

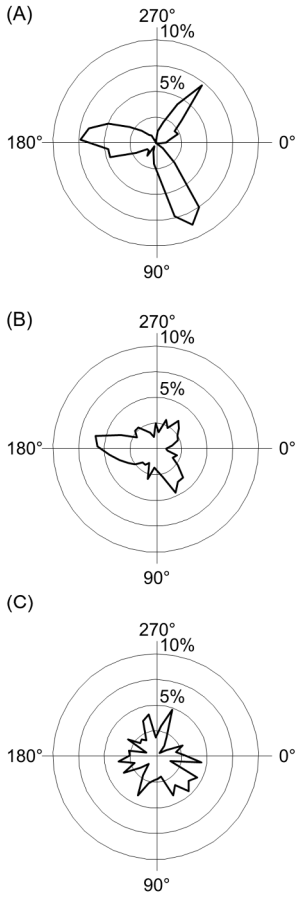

Figure S10. The solvent structure in combination with the Na^+ ions constrains the dihedral angle of the aluminate OH group. The radial extent is the probability density versus dihedral angle as a polar plot, corresponding to the (A) 2.5Å, (B) 6.0 Å, Al-Na^+ distances and, (C) no Na^+.

References:

(1) Reynolds, J. G.; Carter, R.; Felmy, A. R. A Pitzer Interaction Model for the NaNO3–NaNO2–NaOH–H2O System from 0 to 100° C. *Industrial & Engineering Chemistry Research* **2015**, *54,* 3062-3070.

(2) Bénézeth, P.; Hilic, S.; Palmer, D. A. The Solubilities of Gibbsite and Bayerite Below 100° C in Near Neutral to Basic Solutions. *J. Solution Chem.* **2016**, *45,* 1288-1302.

(3) Xiong, Y. A Pitzer model for the Na–Al (OH) 4–Cl–OH system and solubility of boehmite (AlOOH) to high ionic strength and to 250° C. *Chem. Geol.* **2014**, *373,* 37-49.

(4) Weber, C. *Thermodynamic modeling of Savannah River evaporators*; Oak Ridge National Lab., TN (US): 2001.

(5) Wesolowski, D. J. Aluminum speciation and equilibria in aqueous solution: I. The solubility of gibbsite in the system Na-K-Cl-OH-Al $(OH)_4$ from 0 to 100 C. *Geochim. Cosmochim. Acta* **1992**, *56,* 1065-1091.

(6) Königsberger, E.; May, P. M.; Hefter, G. Comprehensive model of synthetic Bayer liquors. Part 3. Sodium aluminate solutions and the solubility of gibbsite and boehmite. *Monatshefte für Chemie/Chemical Monthly* **2006**, *137,* 1139-1149.

(7) Russell, A. S.; Edwards, J. D.; Taylor, C. S. Solubility and density of hydrated aluminas in NaOH solutions. *JOM* **1955**, *7,* 1123-1128.

(8) Holmes, H.; Mesmer, R. Isopiestic molalities for aqueous solutions of the alkali metal hydroxides at elevated temperatures. *The Journal of Chemical Thermodynamics* **1998**, *30,* 311-326.

(9) Simonson, J.; Mesmer, R.; Rogers, P. The enthalpy of dilution and apparent molar heat capacity of NaOH (aq) to 523 K and 40 MPa. *The Journal of Chemical Thermodynamics* **1989**, *21,* 561-584.

(10) Facelli, J. C. Chemical Shift Tensors: Theory and Application to Molecular Structural Problems. *Prog. Nucl. Magn. Reson. Spectrosc.* **2011**, *58*, 176–201.

(11) Facelli, J. C. Chemical Shift Tensors: Theory and Application to Molecular Structural Problems. *Prog. Nucl. Magn. Reson. Spectrosc.* **2011**, *58*, 176–201.